.Human CtIP forms a tetrameric dumbbell-shaped particle which binds and bridges complex DNA end structures for double-strand break repair

SUPPLEMENTARY INFORMATION

Supplementary Discussion 1

Supplementary Figures 1-9

Supplementary Tables 1-3

Supplementary Discussion 1. The putative nuclease activity of CtIP.

It is currently controversial as to whether purified CtIP and its orthologues possess intrinsic nuclease activity (Andres and Williams, 2017). Therefore, to test our CtIP preparations for nuclease activity we incubated CtIP at high concentrations with a forked DNA substrate in the presence of various divalent cations and for extended times (**Supplementary Figure 8**). Nuclease activity was observed which was consistent with cleavage of the 5′-terminated ssDNA flap as reported previously. This nuclease activity may explain the small proportion of less than single contour length substrates observed in our AFM bridging experiments. However, at the highest concentrations tested (which are >>Kd for the binding interaction with the DNA) the half-life of the DNA fork substrate was on the order of several hours. The specific nuclease activity varied between wild type preparations and did not correlate with the ability of CtIP to bind DNA. For example, the C-terminal deletion mutant $CtIP^{1-782}$ does not bind DNA (data not shown) while dephosphorylated CtIP has ~10-fold greater affinity for DNA than wild type (**Figure 4**, main text), but both preparations retain apparent nuclease activity comparable to wild type. Mutations designed to inactivate a putative nuclease active site (N289A and H290A) did reduce the observed nuclease activity in the preparation as reported previously, but a mutation thought to result in hyperactivated nuclease activity (S347D) was less active than any of our wild type preparations (Makharashvili et al., 2014). The dependence of the observed activity on divalent cation identity was qualitatively different for our preparation compared to that reported previously, with Mg^{2+} being the marginally favoured co-factor as opposed to a substantial preference for Mn^{2+} (Makharashvili et al., 2014). Taken together, these observations suggest to us that the nuclease activity in the preparation most likely belongs to a contaminant or co-purified protein rather than to the CtIP polypeptide. However, we are unable to exclude the possibility that CtIP (either as prepared or dephosphorylated) possesses a very weak and/or tightly-regulated nuclease activity.

Supplementary Figure 1. Negative stain electron microscopy.

(A) An example of a micrograph obtained with negative staining of CtIP at 42,000 X magnification. (B) Examples of individual CtIP particles. (C) Further examples of 2D classes for CtIP particles classified as class α or β as indicated.

Supplementary Figure 1. Negative stain electron microscopy.

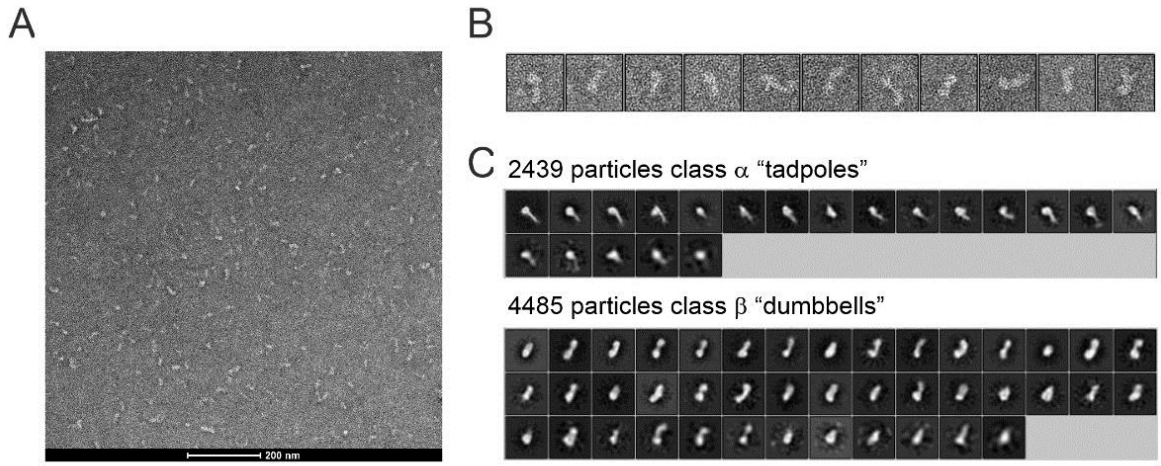

Supplementary Figure 2. Further examples and structural interpretation of AFM particle classes.

Class V particles are thought to represent tetrameric CtIP (see main text and Figure 1D for justification), consisting of a dimer-of-dimers arrangement (blue and red) of parallel coiled coils (zig-zags) meeting at the centre with polar globular domains (circles) that either appear together or in a splayed arrangement. Based on their morphology and relative volume, the cartoons below show speculative interpretations of the other particle classes observed in AFM experiments.

Supplementary Figure 2. Further examples and structural interpretation of AFM particle classes.

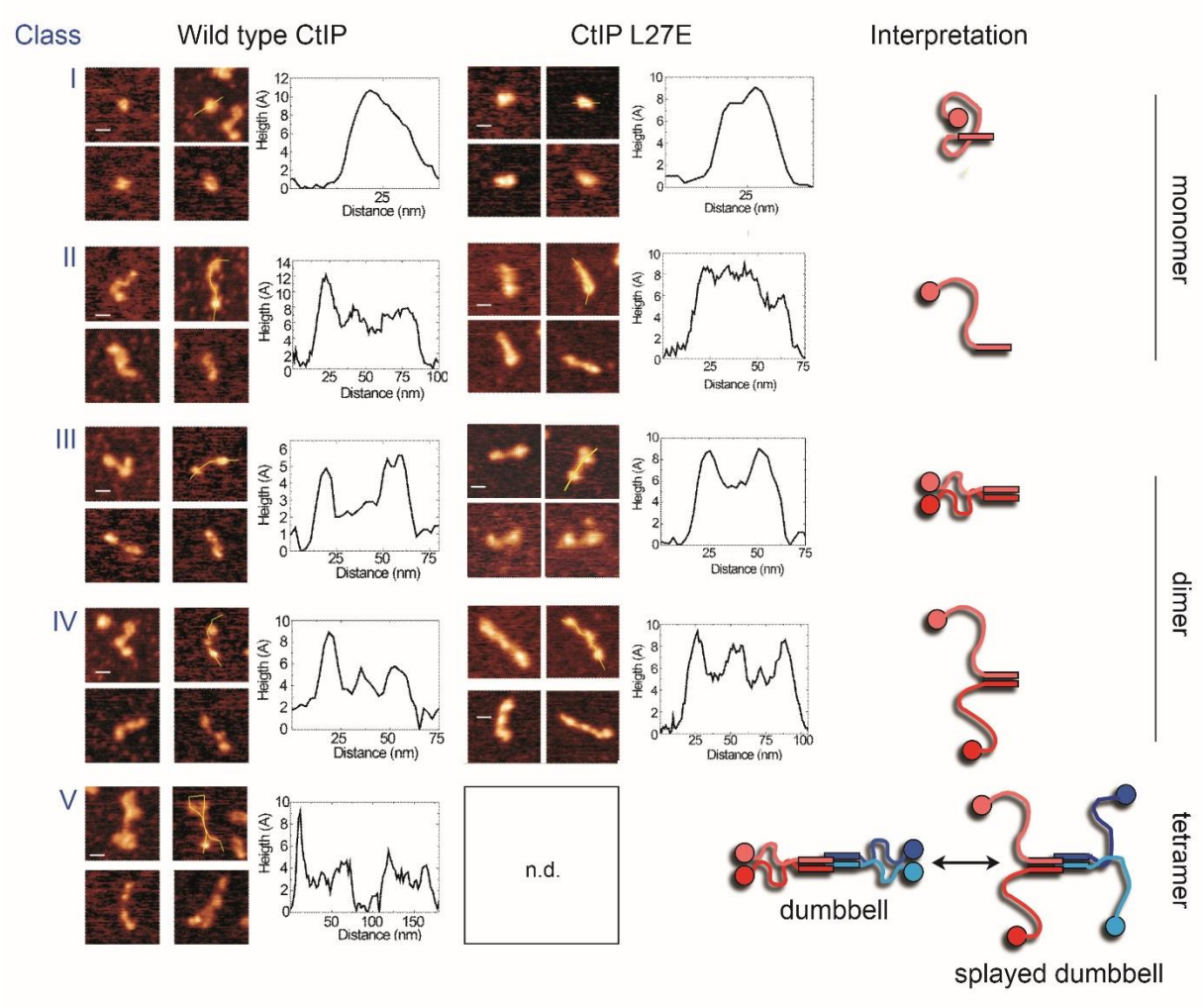

Supplementary Figure 3. The rod between the globular domains is flexible and variable in length.

(A) Examples of CtIP particles displaying significantly different intervening lengths between spots. (B) The distribution of the distances between bright spots in CtIP particles is centred at ~30 nM but is very broad, ranging from <20 to >60 nm. (C) Examples of distance measurements extracted from height profiles for three of the particles shown in A, as indicated by the colouring scheme.

Supplementary Figure 3. The rod between the globular domains is flexible and variable in length.

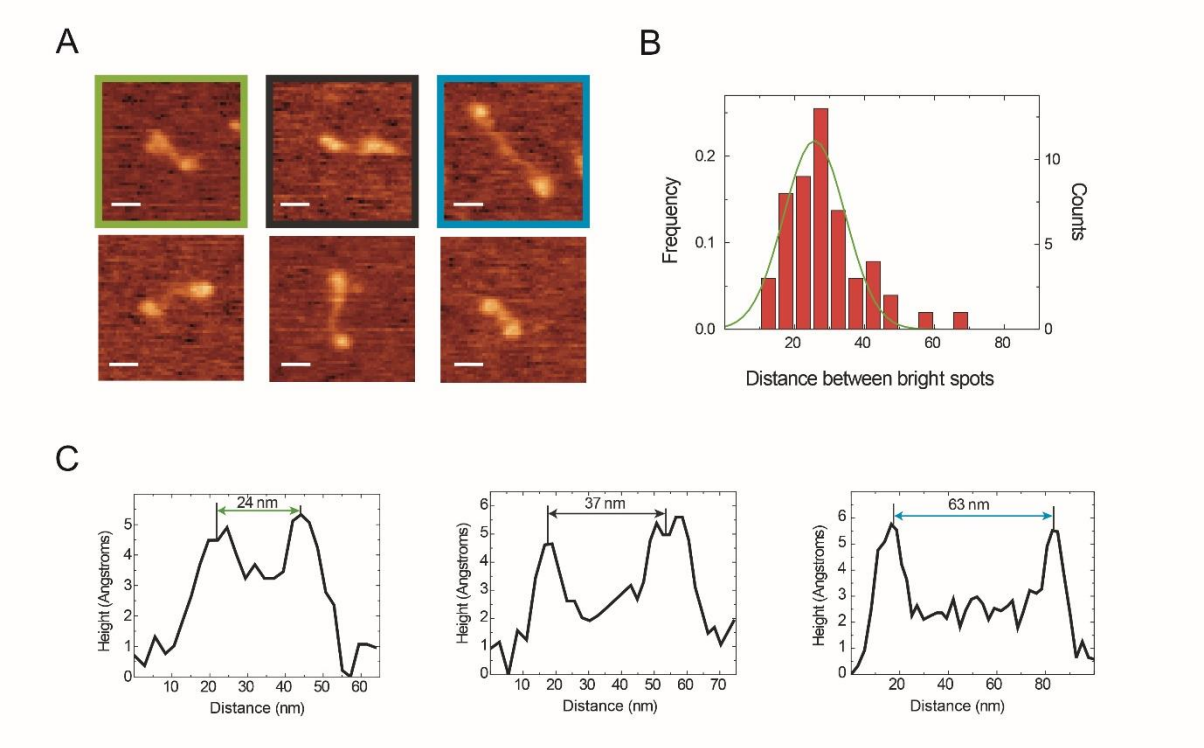

Supplementary Figure 4. CtIP purified from insect cells is hyper-phosphorylated.

Human wild type CtIP was expressed in insect cells, purified in the presence of dephosphorylase inhibitors, and analysed for post-translational modifications by Orbitrap LC-MS/MS mass spectrometry. (A) Coverage of the CtIP polypeptide (91% total) is indicated at different confidence thresholds; less than 1% false discovery rate (green) or less than 5% false discovery rate (yellow). (B) Predicted phosphorylation sites are indicated by the letter P above the CtIP polypeptide at the confidence levels indicated.

Supplementary Figure 4. CtIP purified from insect cells is hyper-phosphorylated.

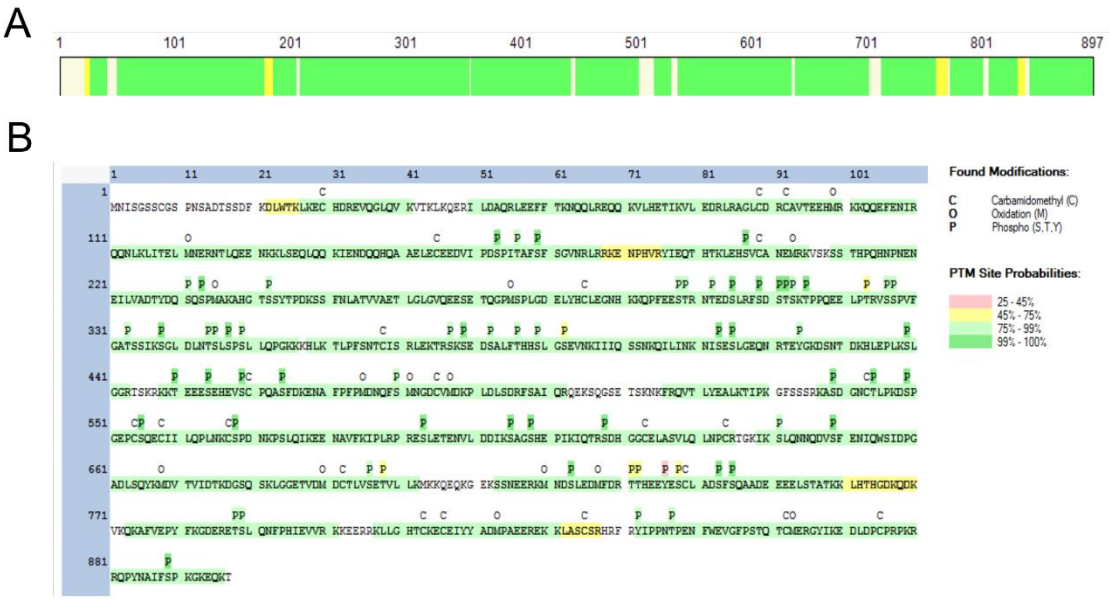

Supplementary Figure 5. Real time measurement of DNA binding potentiation upon treatment of CtIP with λ phosphatase.

(A) Principle of the assay. CtIP (blue) was added to 5 nM HEX-labelled fork DNA (purple) at a concentration equal to ~0.5 x K_d resulting in a low fluorescence anisotropy reading (~0.13). A small volume of λ phosphatase was added to the mixture, resulting in increased anisotropy due to an improved binding affinity. Note that CtIP as prepared in insect cells is hyperphosphorylated and the letter P is intended to represent a phosphorylated amino acid. (B) Representative trace showing potentiation of DNA binding by dephosphorylation of CtIP. The data were well-fitted to a single exponential to yield the half-life shown.

Supplementary Figure 5. Real time measurement of DNA binding potentiation upon treatment of CtIP with λ phosphatase.

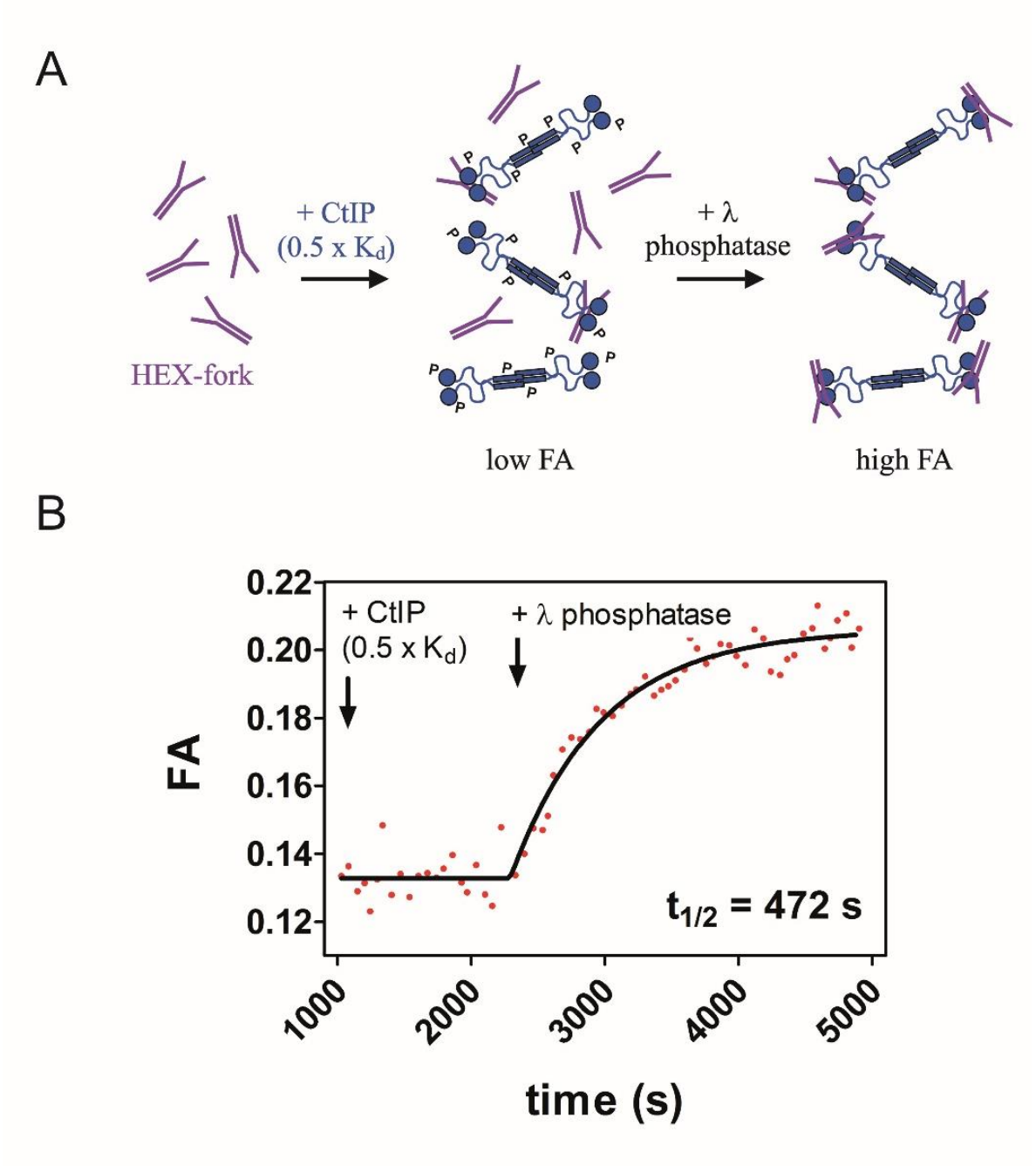

Supplementary Figure 6. Structures of competitor DNA molecules used in this study.

The substrates are numbered as in **Supplementary Table 1**. The arrows represent the 3′-ends of DNA, a yellow circle indicates biotin and the purple square is streptavidin. The blue numbers represent the substrate lengths (in bp or bases) with the exception of substrates 43 and 45, where they represent the number of fragments of the circular DNA they originated from. Substrate 30 may form adopt a circularised structure due to the low persistence length of single-stranded DNA as indicated. For substrate 41, sc indicates that the substrate is supercoiled.

Supplementary Figure 6. Structures of competitor DNA molecules used in this study.

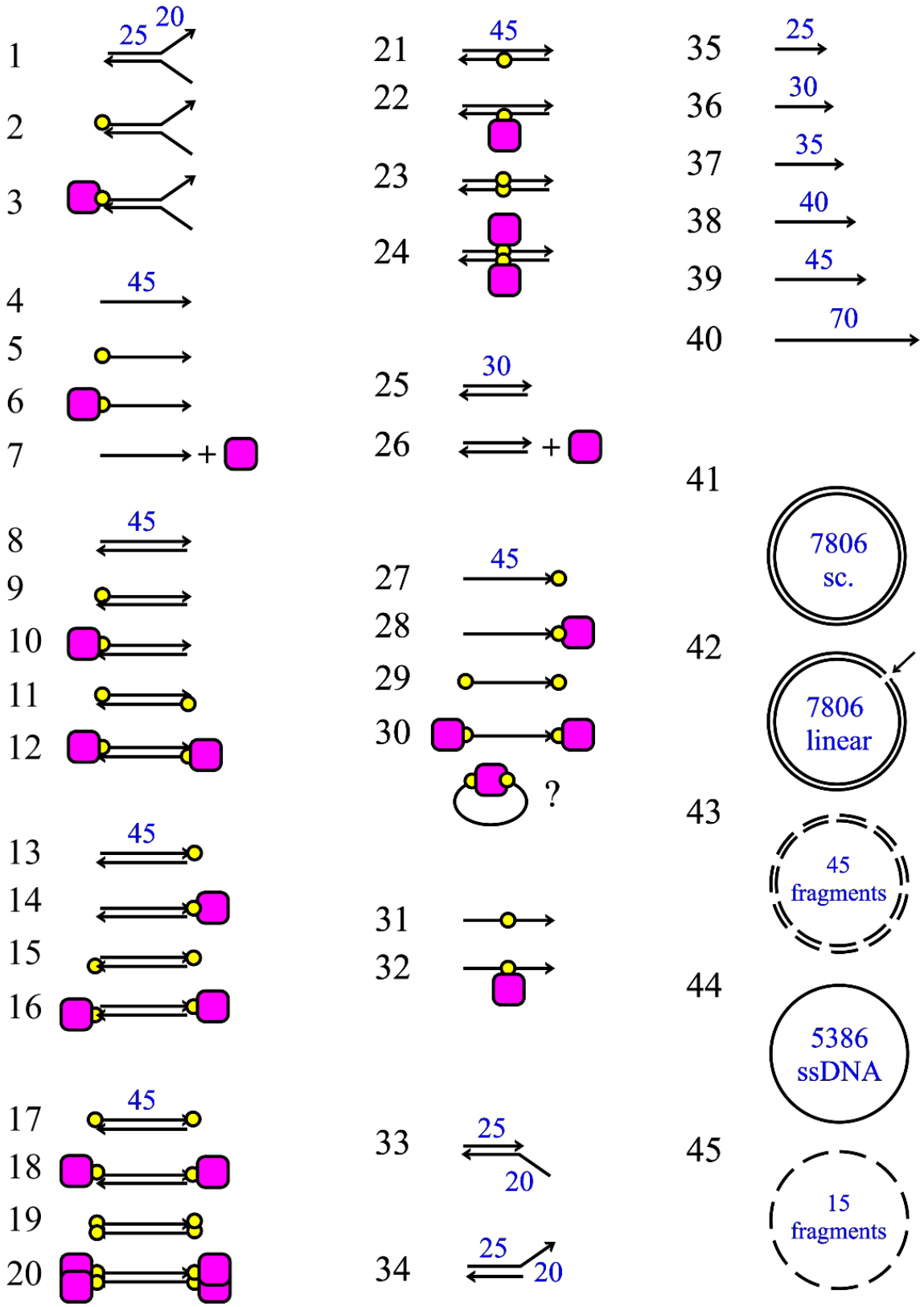

Supplementary Figure 7. IC_{50} values for CtIP binding measured for a wider range of competitor DNA molecules.

(A) Comparison of IC_{50} values for ssDNA molecules of different length as indicated (B) Comparison of how streptavidin binding affects IC_{50} values for duplex DNA molecules containing different numbers and attachment polarities of the biotin moieties (C) Comparison of how streptavidin binding affects IC_{50} values for duplex DNA molecules with biotin in different positions along the duplex (D) Comparison of how streptavidin binding affects IC_{50} values for single-stranded DNA molecules with biotin in different positions. In all figures the arrow represents the 3'-end of the DNA molecule, the yellow circle is biotin, and the purple square is streptavidin.

Supplementary Figure 7. IC_{50} values for CtIP binding measured for a wider range of competitor DNA molecules.

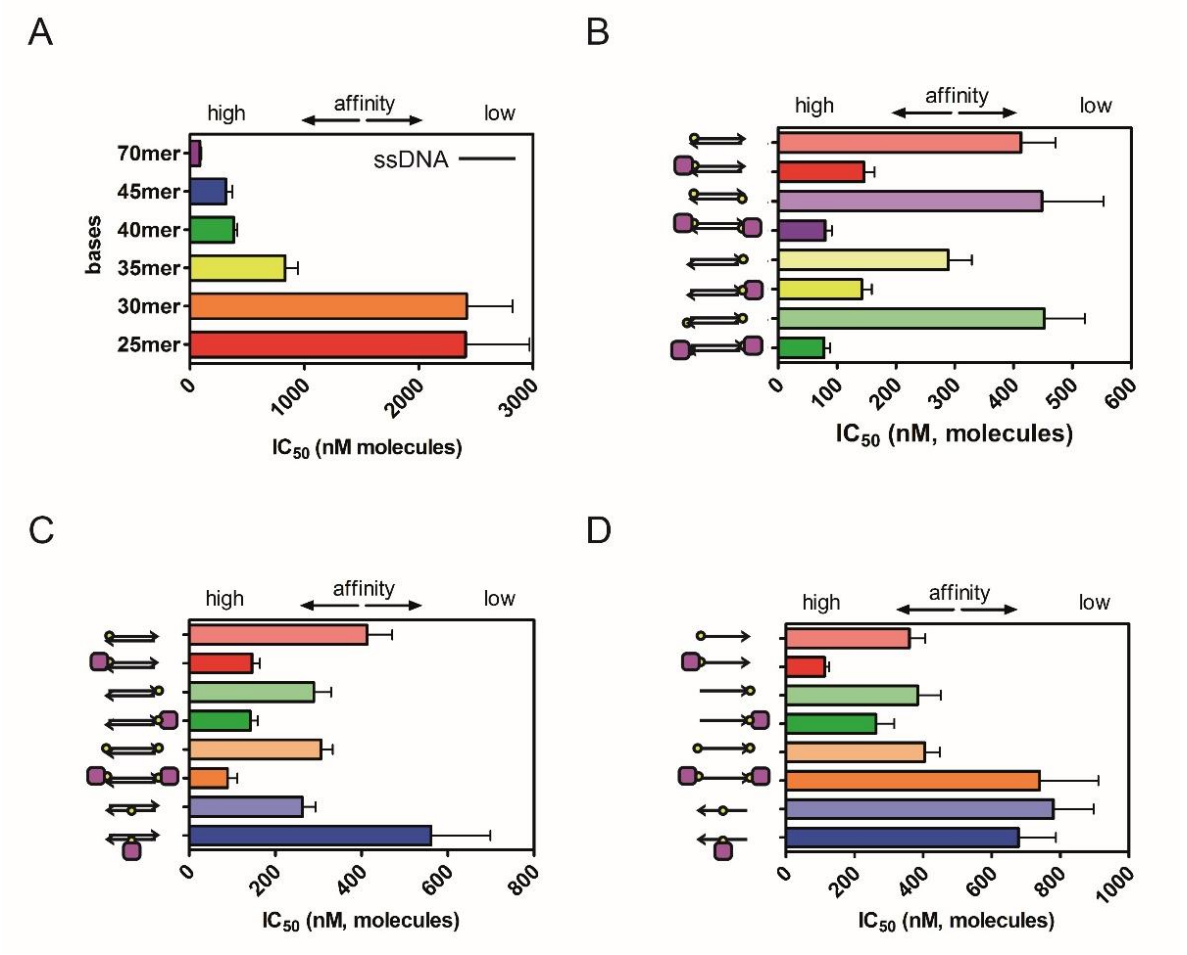

Supplementary Figure 8. Assessment of nuclease activity in CtIP preparations.

(A) Representative nuclease assay for a wild type CtIP preparation (concentrations as indicated in (B)) incubated with 5 nM 5′-Cy5-labelled forked DNA for two hours. (B) Quantified nuclease assays using several different wild type CtIP preparations (labelled A-C) and different CtIP mutants (as indicated) titrated against 5 nM forked DNA. (C) Representative nuclease assay using 250 nM wild type CtIP against 5 nM forked DNA in the presence of different divalent cations. (D) Quantified nuclease assay using 250 nM wild type CtIP against 5 nM forked DNA in the presence of different divalent cations.

Supplementary Figure 8. Assessment of nuclease activity in CtIP preparations.

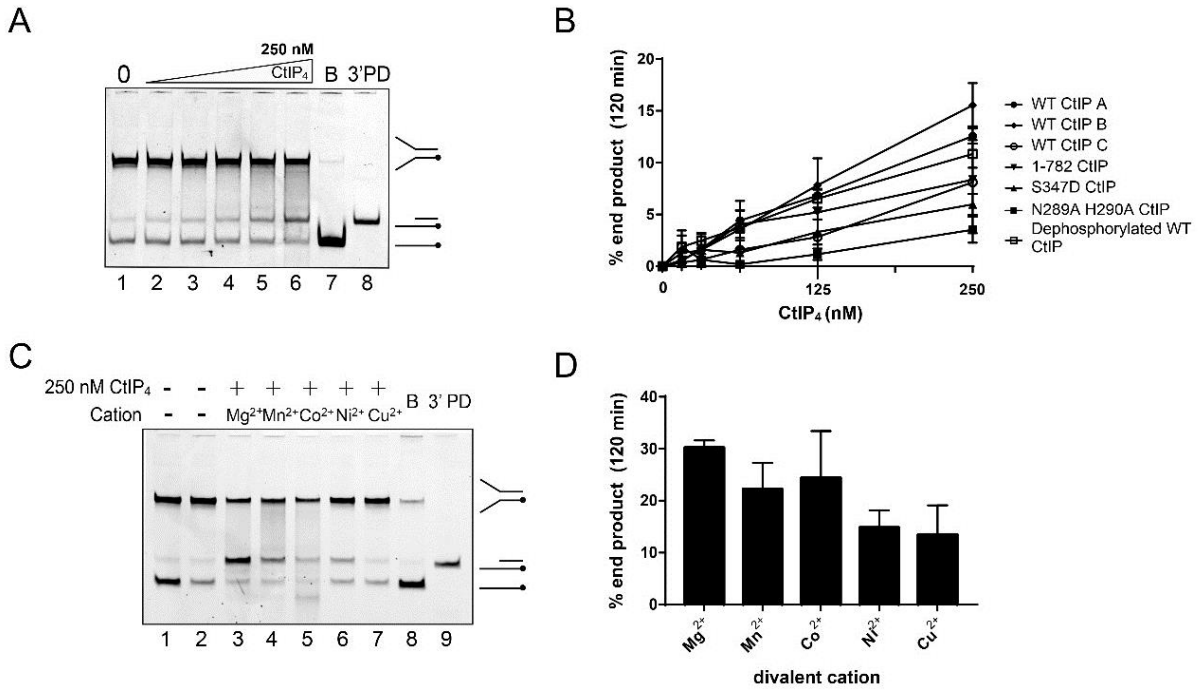

Supplementary Figure 9. CtIP$^{\lambda}$ promotes intermolecular DNA bridging.

(A) Representative AFM images of forked DNA substrates in the absence of CtIP$^{\lambda}$. The contour length histogram shows a single gaussian peak centred on a value equivalent to a single contour length. (B) Representative AFM images of forked DNA substrates in the presence of CtIP$^{\lambda}$. The contour length histogram shows multiples peaks for single-, double-, triple and even quadruple contour length peaks. The solid line shows the gaussian fit for data collected in the absence of CtIP$^{\lambda}$ for comparison. Note that the size of the single-contour peak is substantially reduced.

Supplementary Figure 9. CtIP$^{\lambda}$ promotes intermolecular DNA bridging.

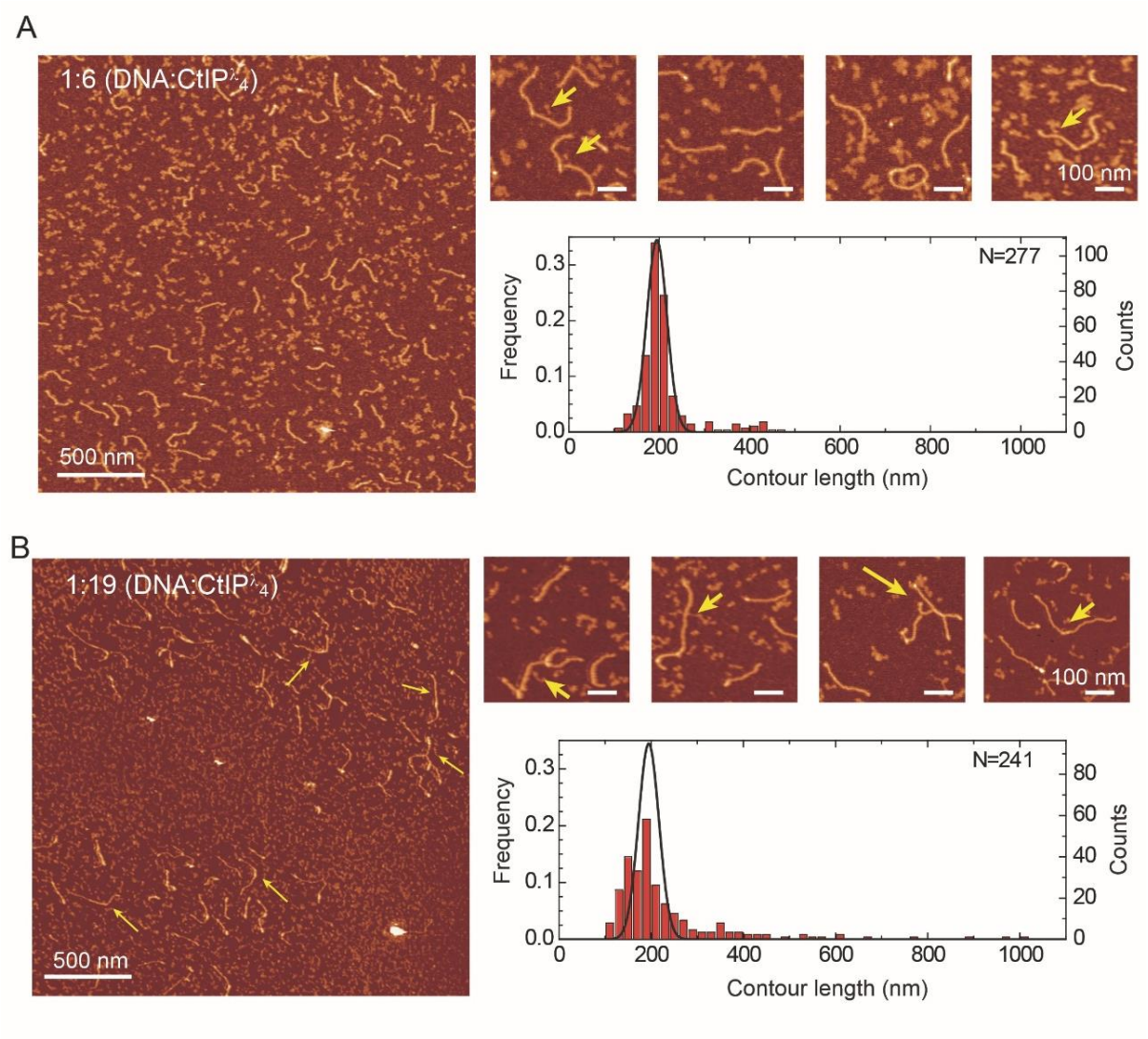

Supplementary Table 1: IC_{50} values for competitor DNA molecules used in DNA unbinding assays. The reported error is the error associated with the fit to a hyperbolic unbinding curve.

#	**DNA Substrate***	**IC_{50}** (nM molecules)	**+/- (nM)**
1	Fork (equivalent to the reference probe DNA)	55	8.7
2	Biotin-Fork	55	6.2
3	Streptavidin-Biotin-Fork	28	4.4
4	ssDNA (45 bases)	314	56
5	Biotin-ssDNA	360	47
6	Streptavidin-Biotin-ssDNA	113	13
7	Streptavidin ssDNA	369	62
8	dsDNA (45 base pairs)	392	44
9	5'-Biotin-dsDNA	413	58
10	Streptavidin-5'-Biotin-dsDNA	146	18
11	Double-5'-Biotin-dsDNA	448	105
12	Double-Streptavidin-5'-Biotin-dsDNA	80	11
13	3'-Biotin-dsDNA	289	40
14	Streptavidin-3'-Biotin-dsDNA	142	17
15	Double-3'-Biotin-dsDNA	452	69
16	Double-Streptavidin-3'-Biotin-dsDNA	78	10
17	5'-3'-Biotin-dsDNA	306	27
18	Streptavidin-5'-3'-Biotin-dsDNA	89	23
19	Double-5'-3'-Biotin-dsDNA	410	36
20	Double-Streptavidin-5'-3'-Biotin-dsDNA	106	15
21	Mid-Biotin dsDNA	263	30
22	Streptavidin-Mid-Biotin-dsDNA	561	138
23	Double-Mid-Biotin dsDNA	229	33
24	Double-Streptavidin-Mid-Biotin-dsDNA	261	42
25	dsDNA (30 base pairs)	915	118
26	Streptavidin dsDNA	861	159
27	3'-Biotin-ssDNA	384	68
28	Strepatavidin-3'-Biotin-ssDNA	263	53
29	5'-3'-Biotin-ssDNA	405	44
30	Streptavidin-5'-3'-Biotin-ssDNA	740	171
31	Mid-Biotin-ssDNA	780	117
32	Streptavidin-Mid-Biotin-ssDNA	678	109

33	5'-overhang	346	47
34	3'-overhang	305	47
35	ssDNA (25 bases)	2410	560
36	ssDNA (30 bases)	2419	403
37	ssDNA (35 bases)	831	113
38	ssDNA (40 bases)	380	34
39	ssDNA (45 bases)	314	56
40	ssDNA (70 bases)	86	13
41	plasmid dsDNA (pSP73 JY10) supercoiled	0.54 (4140 nM ntd)	0.046 360
42	plasmid dsDNA (pSP73 JY10) linear	0.45 (3465 nM ntd)	0.058 450
43	plasmid dsDNA (pSP73 JY10) 45 fragments	0.63 (4860 nM ntd)	0.064 495
44	φX174 virion ssDNA circular	0.53 (2880 nM ntd)	11 495
45	φX174 virion ssDNA 15 fragments	0.51 (2745 nM ntd)	0.046 360

* The constituent oligonucleotides for these DNA substrates are shown in **Supplementary Tables 2 and 3**.

Supplementary Table 2: Assembly/Source of DNA substrates. Small DNA substrates were prepared by annealing different combinations of short oligonucleotides (A-T). The sequences for the oligonucleotides are presented in Supplementary Table 3.

#	**DNA Substrate**	**Constituent oligos / source (see also Table 3)**
1	Fork (equivalent to the reference probe DNA)	A + B
2	Biotin-Fork	B + C
3	Streptavidin-Biotin-Fork	B + C
4	ssDNA (45 bases)	D
5	Biotin-ssDNA	E
6	Streptavidin-Biotin-ssDNA	E
7	Streptavidin ssDNA	D
8	dsDNA (45 base pairs)	D + F
9	5'-Biotin-dsDNA	E + F
10	Streptavidin-5'-Biotin-dsDNA	E + F
11	Double-5'-Biotin-dsDNA	E + G
12	Double-Streptavidin-5'-Biotin-dsDNA	E + G
13	3'-Biotin-dsDNA	F + H
14	Streptavidin-3'-Biotin-dsDNA	F + H
15	Double-3'-Biotin-dsDNA	H + I
16	Double-Streptavidin-3'-Biotin-dsDNA	H + I
17	5'-3'-Biotin-dsDNA	F + J
18	Streptavidin-5'-3'-Biotin-dsDNA	F + J
19	Double-5'-3'-Biotin-dsDNA	J + K
20	Double-Streptavidin-5'-3'-Biotin-dsDNA	J + K
21	Mid-Biotin dsDNA	F + L
22	Streptavidin-Mid-Biotin-dsDNA	F + L
23	Double-Mid-Biotin dsDNA	L + M
24	Double-Streptavidin-Mid-Biotin-dsDNA	L + M
25	dsDNA (25 base pairs)	N + O
26	Streptavidin dsDNA	N + O
27	3'-Biotin-ssDNA	H
28	Strepatavidin-3'-Biotin-ssDNA	H
29	5'-3'-Biotin-ssDNA	J
30	Streptavidin-5'-3'-Biotin-ssDNA	J
31	Mid-Biotin-ssDNA	L

32	Streptavidin-Mid-Biotin-ssDNA	L
33	5'-overhang	F + N
34	3'-overhang	D + O
35	ssDNA (25 bases)	P
36	ssDNA (30 bases)	Q
37	ssDNA (35 bases)	R
38	ssDNA (40 bases)	S
39	ssDNA (45 bases)	D
40	ssDNA (70 bases)	T
41	plasmid dsDNA (pSP73 JY10) supercoiled	Ref (Yeeles et al., 2011)
42	plasmid dsDNA (pSP73 JY10) linear	Ref (Yeeles et al., 2011)
43	plasmid dsDNA (pSP73 JY10) 45 fragments	Ref (Yeeles et al., 2011)
44	φX174 virion ssDNA circular	New England Biolabs
45	φX174 virion ssDNA 15 fragments	New England Biolabs

Supplementary Table 3: Sequences of oligonucleotides used to assemble competitor DNA molecules

Constituent Oligonucleotide	Sequence (5'-3')
A	GCT TGC TAG GAC GGA TCG CTC GAG GTT TTT TTT TTT TTT TTT TTT
B	TTT TTT TTT TTT TTT TTT TTC CTC GAG CGA TCC GTC CTA GCA AGC
C	Biotin-GCT TGC TAG GAC GGA TCG CTC GAG GTT TTT TTT TTT TTT TTT TTT
D	GCT TGC TAG GAC GGA TCG CTC GAG GTT TAC CCT GCT ATA CGG TGA
E	Biotin-GCT TGC TAG GAC GGA TCG CTC GAG GTT TAC CCT GCT ATA CGG TGA
F	TCA CCG TAT AGC AGG GTA AAC CTC GAG CGA TCC GTC CTA GCA AGC
G	Biotin-TCA CCG TAT AGC AGG GTA AAC CTC GAG CGA TCC GTC CTA GCA AGC
H	GCT TGC TAG GAC GGA TCG CTC GAG GTT TAC CCT GCT ATA CGG TGA-Biotin
I	TCA CCG TAT AGC AGG GTA AAC CTC GAG CGA TCC GTC CTA GCA AGC-Biotin
J	Biotin-GCT TGC TAG GAC GGA TCG CTC GAG GTT TAC CCT GCT ATA CGG TGA-Biotin
K	Biotin-TCA CCG TAT AGC AGG GTA AAC CTC GAG CGA TCC GTC CTA GCA AGC-Biotin
L	GCT TGC TAG GAC GGA TCG C dT-Biotin C GAG GTT TAC CCT GCT ATA CGG TGA
M	TCA CCG TAT AGC AGG GTA AAC C dT-Biotin C GAG CGA TCC GTC CTA GCA AGC
N	GCT TGC TAG GAC GGA TCG CTC GAG G
O	C CTC GAG CGA TCC GTC CTA GCA AGC
P	GAG ATA TAC ATA TGA AAA CGC CGT G
Q	GCG TAA GCC CCG GGA TGG CTA AAG GCC TTG
R	GTT TGT TGT CCT TGA CCA AGT AGA GGC TGC GCT CG
S	GGA TTA CCG CTG TGA ATG GGC TTC GTT TTA CGA TTA TTG T
T	TTT TTT TTT TTT TTT TTT TTT TTT TTT TTT TTT TTT TTT TTT TTT TTT TTT TTT TTT TTT TTT TTT T

References

Andres, S.N., and Williams, R.S. (2017). CtIP/Ctp1/Sae2, molecular form fit for function. DNA Repair (Amst) *56*, 109-117.

Makharashvili, N., Tubbs, A.T., Yang, S.H., Wang, H., Barton, O., Zhou, Y., Deshpande, R.A., Lee, J.H., Lobrich, M., Sleckman, B.P., *et al.* (2014). Catalytic and noncatalytic roles of the CtIP endonuclease in double-strand break end resection. Mol Cell *54*, 1022-1033.

Yeeles, J.T., van Aelst, K., Dillingham, M.S., and Moreno-Herrero, F. (2011). Recombination hotspots and single-stranded DNA binding proteins couple DNA translocation to DNA unwinding by the AddAB helicase-nuclease. Mol Cell *42*, 806-816.